



1 **A mechanistic model of an upper bound on oceanic carbon export as**
2 **a function of mixed layer depth and temperature**

3 Zuchuan Li^{1*}, Nicolas Cassar¹

4 ¹Division of Earth and Ocean Sciences, Nicholas School of the Environment, Duke University,
5 Durham, North Carolina, USA

6 * Correspondence to: Zuchuan Li (zuchuan.li@duke.edu)

7

8 **Abstract**

9 Export production reflects the amount of organic matter transferred from the surface ocean to
10 depth through biological processes. This export is in great part controlled by nutrient and light
11 availability, which are conditioned by mixed layer depth (MLD). In this study, building on
12 Sverdrup's critical depth hypothesis, we derive a mechanistic model of an upper bound on
13 carbon export based on the metabolic balance between photosynthesis and respiration as a
14 function of MLD and temperature. We find that the upper bound is a positively skewed bell-
15 shaped function of MLD. Specifically, the upper bound increases with deepening mixed layers
16 down to a critical depth, beyond which a long tail of decreasing carbon export is associated with
17 increasing heterotrophic activity and decreasing light availability. We also show that in cold
18 regions the upper bound on carbon export decreases with increasing temperature when mixed
19 layers are deep, but increases with temperature when mixed layers are shallow. A metaanalysis
20 shows that our model envelopes field estimates of carbon export from the mixed layer. When
21 compared to satellite export production estimates, our model indicates that export production in
22 some regions of the Southern Ocean, most particularly the Subantarctic Zone, is likely limited by
23 light for a significant portion of the growing season.

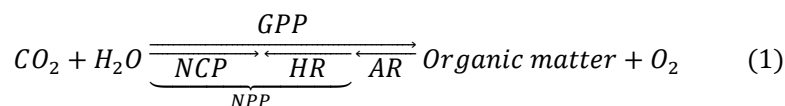
24



25 1. Introduction

26 Photosynthesis in excess of respiration at the ocean surface leads to the production of organic
 27 matter, part of which is transported to the deep ocean through sinking and mixing [*Volk and*
 28 *Hoffert, 1985*]. This biological process, known as export production (aka soft tissue biological
 29 carbon pump) lowers carbon dioxide (CO₂) concentrations at the ocean surface and facilitates the
 30 flux of CO₂ from the atmosphere into the ocean.

31 Export production is a function of net community production (NCP) which is defined as the
 32 balance between net primary production (NPP) and heterotrophic respiration (HR), or the
 33 difference between gross primary production (GPP) and community respiration (CR; HR plus
 34 autotrophic respiration (AR)) (the acronyms used in this study are presented in Table 1):



$$Export\ production = NCP - MLD \times \frac{d(POC + DOC)}{dt} \quad (2)$$

35 where POC, DOC and MLD represent particulate organic carbon, dissolved organic carbon and
 36 mixed layer depth, respectively. If the organic carbon inventory (POC+DOC) in the mixed layer
 37 is at steady state, NCP is equal to export production (equation (2)). Without allochthonous
 38 sources of organic matter, if the organic matter inventory in the mixed layer decreases, NCP will
 39 be predicted to be transiently smaller than export production. Conversely, export may lag NPP
 40 [*Henson et al., 2015; Stange et al., 2017*], in which case NCP is expected to be greater than
 41 export production.

42 We define the upper bound on carbon export (NCP^*) from the mixed layer as the maximum
 43 export achievable should all limiting factors other than light (e.g., nutrients) be alleviated. Light
 44 availability exponentially decays with depth due to absorption by water and its constituents. The



45 mixing of phytoplankton to depth therefore impacts phytoplankton physiology and productivity
46 [Cullen and Lewis, 1988; Lewis *et al.*, 1984], with the depth-integrated NPP expected to increase
47 down to the euphotic depth. Respiration, on the other hand, is often modeled to be some function
48 of organic matter concentration, which is expected to be constant with depth if homogeneously
49 mixed within the mixed layer. Temperature is also believed to be an important control on carbon
50 export because respiration is more temperature-sensitive than photosynthesis [Laws *et al.*, 2000;
51 Lopez-Urrutia *et al.*, 2006; Rivkin and Legendre, 2001]. Field observations confirm that NCP is
52 generally lower at high temperatures and consistently low when mixed layers are deep. These
53 patterns have been attributed to the balance between depth-integrated photosynthesis and
54 respiration as a function of MLD and temperature [Cassar *et al.*, 2011; Eveleth *et al.*, 2016;
55 Huang *et al.*, 2012; Shadwick *et al.*, 2015; Tortell *et al.*, 2015]. However, descriptions of the
56 underlying mechanisms heretofore remain qualitative.

57 In his seminal paper, Sverdrup presented an elegant model to demonstrate that vernal
58 phytoplankton blooms (i.e., organic matter accumulation at the ocean surface) may be driven by
59 increased light availability when the MLD shoals above a critical depth (Z_c) [Sverdrup, 1953]. In
60 our study, we build upon Sverdrup [1953] and derive a mechanistic model of an upper bound on
61 carbon export with respect to MLD, temperature, photosynthetically active radiation (PAR),
62 phytoplankton maximum growth rate (μ_{max}), and heterotrophic activity. We compare our NCP^*
63 model to observations, and use this model in conjunction with satellite export production
64 estimates to identify regions in the world's oceans where light may limit export production.

65 **2. Model description and comparison to observations**

66 **2.1. Net community production and light availability**



67 A conceptual representation of the metabolic balance between volumetric NCP, NPP, and
 68 HR profiles is presented in Figure 1(A). According to equation (1), the volumetric NCP flux at a
 69 given depth (z) in the mixed layer results from the difference between volumetric NPP and HR:

$$NCP(z) = NPP(z) - HR(z) \quad (3)$$

70 where z increases with depth. $NPP(z)$ is a function of the autotroph's intrinsic growth rate
 71 (μ) times their biomass concentration (C). Assuming that the effect of nutrients and light on
 72 photosynthetic rates abides by Michaelis-Menten kinetics, and neglecting the effect of
 73 photoinhibition [Dutkiewicz *et al.*, 2001; Huisman and Weissing, 1994], $NPP(z)$ may be
 74 expressed as follows:

$$NPP(z) = \mu(z) \times C = \frac{N}{N + k_m^N} \times \frac{I(z)}{I(z) + k_m^I} \times \mu_{max} \times C \quad (4)$$

75 where μ_{max} is the maximum intrinsic growth rate of the autotrophic community; N and k_m^N
 76 represent the nutrient concentration and half-saturation constant, respectively; and I and k_m^I
 77 represent the irradiance level and half-saturation constant, respectively. μ_{max} , N , k_m^N , k_m^I and C
 78 are assumed to be well mixed within the mixed layer. The first two terms on the right-hand side
 79 of equation (4) account for the effect of nutrient and light availability on autotrophic growth rates,
 80 and they are hereafter defined as follows for simplicity:

$$N_m = \frac{N}{N + k_m^N} \quad (5a)$$

$$I_m(z) = \frac{I(z)}{I(z) + k_m^I} \quad (5b)$$

81 $I(z)$ is modeled as an exponential decay of PAR just beneath the water surface (I_0):

$$I(z) = I_0 \times e^{-K_I \times z} \quad (6)$$



82 where K_I is diffusion attenuation coefficient which is assumed to be independent of depth in the
 83 mixed layer.

84 As a first approximation, we assume that $HR(z)$ is proportional to C as in previous studies
 85 [*Dutkiewicz et al.*, 2001; *Huisman and Weissing*, 1994; *Rivkin and Legendre*, 2001; *Sverdrup*,
 86 1953; *White et al.*, 1991]:

$$HR(z) = r_{HR} \times C \quad (7)$$

87 where r_{HR} represents the intrinsic heterotrophic respiration rate which is assumed to be
 88 dependent on temperature (see below), and independent of depth. In reality, $HR(z)$ is likely best
 89 modeled as a function of the concentration of labile organic matter — an additional term could
 90 be included to account for the relationship of total labile organic matter to C .

91 NCP integrated over the mixed layer ($NCP(0, MLD)$) can be derived from equations (3-7):

$$\begin{aligned} NCP(0, MLD) &= NPP(0, MLD) - HR(0, MLD) \\ &= \int_0^{MLD} NPP(z) dz - \int_0^{MLD} HR(z) dz \\ &= N_m \times I_m(0, MLD) \times \mu_{max} \times C - r_{HR} \times MLD \times C \end{aligned} \quad (8)$$

92 The first term on the right side of equation (8) represents NPP integrated over the mixed layer
 93 ($NPP(0, MLD)$), which is equivalent to the product of $\int_0^{MLD} \mu(z) dz$ and C , where the former
 94 term is modeled to be a function of μ_{max} conditioned by nutrient and light availability within the
 95 mixed layer. $I_m(0, MLD)$ can be derived as follows:

$$I_m(0, MLD) = \int_0^{MLD} I_m(z) dz = -\frac{1}{K_I} \times \ln \left(\frac{I_0 \times e^{-K_I \times MLD} + k_m^I}{I_0 + k_m^I} \right) \quad (9)$$

96 NCP integrated over the mixed layer (equation (8)) is a bell-shaped function of MLD as depicted
 97 in the schematic diagram of Figure 1(B).

98 2.2. Net community production and phytoplankton biomass concentration



99 As can be seen from equation (8), $NCP(0,MLD)$ is a direct function of C because
 100 $NPP(0,MLD)$ and $HR(0,MLD)$ are proportional to C . $NCP(0,MLD)$ is also an indirect function
 101 of C due its effect on light attenuation (i.e., K_I). The attenuation coefficient K_I can be divided
 102 into water and non-water components ($K_I = K_I^w + K_I^{nw}$) [Baker and Smith, 1982; Smith and
 103 Baker, 1978a; b], where K_I^{nw} is controlled by the concentrations of phytoplankton, colored
 104 dissolved organic matter (CDOM), and non-algal particles (NAP). In the open ocean where
 105 CDOM and NAP co-vary with phytoplankton [Morel and Prieur, 1977], K_I can be related to C
 106 as follows:

$$K_I = K_I^w + k_c \times C \quad (10)$$

107 where k_c is a function of the solar zenith angle, the specific absorption and backscattering
 108 coefficients of phytoplankton, and the relationship between phytoplankton, CDOM, and NAP.

109 To calculate how $NCP(0,MLD)$ varies as a function of C , we examine its first ($\frac{dNCP(0,MLD)}{dC}$)
 110 and second ($\frac{d^2NCP(0,MLD)}{dC^2}$) derivatives with respect to C based on equations (8) and (10):

$$\begin{aligned} & \frac{dNCP(0,MLD)}{dC} \\ &= N_m \times \mu_{max} \times \frac{K_I^w \times I_m(0,MLD) + k_c \times C \times MLD \times I_m(MLD)}{K_I^w + k_c \times C} - r_{HR} \times MLD \end{aligned} \quad (11)$$

$$\begin{aligned} & \frac{d^2NCP(0,MLD)}{dC^2} = N_m \times k_c \times \frac{\mu_{max}}{K_I} \\ & \times \left\{ \frac{2 \times K_I^w}{K_I} \times (MLD \times I_m(MLD) - I_m(0,MLD)) - \frac{k_c \times C \times I_m(MLD)^2 \times MLD^2 \times k_m^l}{I_0 \times e^{-K_I \times MLD}} \right\} \end{aligned} \quad (12)$$

111 when $MLD > 0$, $I_m(0,MLD) > MLD \times I_m(MLD)$:



$$\begin{aligned}
 I_m(0, MLD) &= \int_0^{MLD} \frac{I_0 \times e^{-K_I \times z}}{I_0 \times e^{-K_I \times z} + k_m^I} dz \\
 &> \int_0^{MLD} \frac{I_0 \times e^{-K_I \times MLD}}{I_0 \times e^{-K_I \times MLD} + k_m^I} dz = MLD \times I_m(MLD) \quad (13)
 \end{aligned}$$

112 The detailed derivation of equations (11-12) can be found in the supplementary material.
 113 Substituting the inequality (13) into equation (12) gives $\frac{d^2 NPP(0, MLD)}{dC^2} < 0$, which suggests that
 114 $\frac{dNCP(0, MLD)}{dC}$ decreases with increasing C reaching an asymptote of $\lim_{C \rightarrow \infty} \left(\frac{dNCP(0, MLD)}{dC} \right) = -r_{HR} \times$
 115 $MLD < 0$ (Figure 2(B)). Additionally, because $NCP(0, MLD)$ must be nil when there is no
 116 autotrophic biomass ($NCP(0, MLD)|_{C=0} = 0$), $\lim_{C \rightarrow 0} \left(\frac{dNCP(0, MLD)}{dC} \right)$ must be larger than 0, otherwise
 117 the ecosystem would be net heterotrophic which is unachievable without an allochthonous source
 118 of organic matter. $\lim_{C \rightarrow 0} \left(\frac{dNCP(0, MLD)}{dC} \right) > 0$ and $\lim_{C \rightarrow \infty} \left(\frac{dNCP(0, MLD)}{dC} \right) = -r_{HR} \times MLD < 0$ suggest the
 119 existence of $\left. \frac{dNCP(0, MLD)}{dC} \right|_{C=C^*} = 0$ where C^* corresponds to an autotrophic biomass concentration
 120 which maximizes $NCP(0, MLD)$ (i.e., NCP^*).

121 The dependence of $NCP(0, MLD)$ on C can be conceptually understood in the following way.
 122 Given a water column with sufficient nutrients, the critical depth Z_c and compensation depth Z_p
 123 are expected to shoal as C increases. When C is low, $NCP(0, MLD)$ increases with C because of
 124 its greater impact on $NPP(0, MLD)$ than on $HR(0, MLD)$. As C further increases, the increase in
 125 $NPP(0, MLD)$ with C slows because of light attenuation (i.e., K_I). There is therefore a C^* which
 126 maximizes the difference between $NPP(0, MLD)$ and $HR(0, MLD)$ leading to NCP^* (Figure 2).
 127 Beyond this point (C^*), further increasing C will cause self-shading and limit photosynthesis in
 128 the deep part of the mixed layer, as a result decreasing $NCP(0, MLD)$. Beyond a critical biomass



129 (C_c), the ecosystem becomes net heterotrophic. Without an allochthonous source of organic
 130 carbon, this is only transiently sustainable.

131 **2.3. Mixed layer depth and compensation depth**

132 By definition, if $NCP(MLD)$ is smaller than 0 (i.e., net heterotrophy at the bottom of the
 133 mixed layer), the MLD must be deeper than Z_p ($MLD > Z_p$) (and vice versa). To determine the
 134 sign of $NCP(MLD)$, we substitute inequality (13) into equation (11). According to the inequality
 135 presented in equation (13), $\frac{K_l^w \times I_m(0,MLD) + k_c \times C \times MLD \times I_m(MLD)}{K_l^w + k_c \times C}$ in equation (11) must be larger than
 136 $\frac{K_l^w \times MLD \times I_m(MLD) + k_c \times C \times MLD \times I_m(MLD)}{K_l^w + k_c \times C}$ (which is equal to $MLD \times I_m(MLD)$). After simple
 137 rearrangements, the substitution of inequality (13) into equation (11) leads to:

$$\frac{dNCP(0,MLD)}{dC} > MLD \times (N_m \times I_m(MLD) \times \mu_{max} - r_{HR}) = \frac{MLD}{C} \times NCP(MLD) \quad (14)$$

138 The inequality in equation (14) in turn suggests that when $NCP(0,MLD)$ is maximized
 139 ($\frac{dNCP(0,MLD)}{dC} = 0$), $NCP(MLD)$ is negative (net heterotrophic) and hence the MLD is deeper than
 140 Z_p ($MLD > Z_p$). This counterintuitive result is attributable both to the uneven distribution of
 141 light availability in the water column (equation (13)) and to water which absorbs light but does
 142 not contribute to biomass accumulation. When the mixed layer is at the Z_p , a slight increase in C
 143 will leads to negative $NCP(MLD)$ due to decreasing light availability at the base of mixed layer,
 144 but will increase NCP higher in the water column because of the increase in biomass. The
 145 increase in NCP in the shallow parts of the mixed layer therefore overcompensates for the net
 146 heterotrophy at the bottom of the mixed layer, thus maximizing the depth-integrated NCP. If
 147 light were uniformly distributed in the water column (i.e., $I_m(0,MLD) = MLD \times I_m(MLD)$) and



148 if water did not attenuate light ($K_I^w = 0$ in equation (11)), $MLD = Z_p$ would maximize
 149 $NCP(0, MLD)$, which is consistent with *Huisman and Weissing* [1994].

150 2.4. An upper bound on carbon export

151 Equations (11-13) delineate the conditions for an upper bound on carbon export (NCP^*). In
 152 order to simplify the relationship of NCP^* to MLD and temperature, we approximate

153 $I_m(0, MLD)$:

$$\begin{aligned}
 I_m(0, MLD) &= -\frac{1}{K_I} \times \ln \left(1 + \frac{I_0}{I_0 + k_m^I} \times (e^{-K_I \times MLD} - 1) \right) \\
 &\approx I_m(0) \times \frac{1 - e^{-K_I \times MLD}}{K_I} \\
 &\approx I_m(0) \times \frac{1}{K_I} \quad (15)
 \end{aligned}$$

154 where $I_m(0) = \frac{I_0}{I_0 + k_m^I}$. Based on equation (15), $NCP(0, MLD)$ in equation (8) can be
 155 approximated as:

$$NCP(0, MLD) = C \times MLD \times \left(\frac{1}{K_I \times MLD} \times \mu^* - r_{HR} \right) \quad (16)$$

156 where $\mu^* = I_m(0) \times N_m \times \mu_{max}$.

157 We first need to derive the C^* which maximizes $NCP(0, MLD)$ (i.e., NCP^*) in equation (16).

158 C^* can be solved from the first derivative of $NCP(0, MLD)$ in equation (16) with respect to C :

$$\left. \frac{dNCP(0, MLD)}{dC} \right|_{NCP(0, MLD)=NCP^*} = \mu^* \times \frac{K_I^w}{(k_c \times C^* + K_I^w)^2} - MLD \times r_{HR} = 0 \quad (17)$$

159

160 and therefore:

$$C^* = \frac{1}{k_c} \times \left[-K_I^w + \sqrt{\frac{\mu^* \times K_I^w}{MLD \times r_{HR}}} \right] \quad (18)$$



162 Equation (18) decreases with MLD. As C^* is positive ($C^* \geq 0$) and cannot go to infinity
 163 ($C^* \leq C_{max}^*$), MLD should satisfy $MLD_{C_{max}^*} \leq MLD \leq \frac{\mu^*}{r_{HR} \times K_I^w}$, where $MLD_{C_{max}^*}$ represents the
 164 MLD corresponding to the maximum achievable autotroph's biomass concentration (C_{max}^*) in
 165 the surface ocean. Substituting C^* from equation (18) into equation (16):

$$\sqrt{NCP^*} = a_2 \times \sqrt{I_m(0)} + a_1 \times \sqrt{MLD} \quad (19)$$

166 where $a_1 = -\sqrt{\frac{K_I^w \times r_{HR}}{k_c}}$ and $a_2 = \sqrt{\frac{N_m \times \mu_{max}}{k_c}}$. Constants a_1 and a_2 are functions of r_{HR} and μ_{max} ,
 167 respectively, which are generally modeled to increase with temperature (T) [Eppley, 1972; Rivkin
 168 and Legendre, 2001]:

$$\mu_{max} \propto e^{P_t \times T} \quad (20a)$$

$$r_{HR} \propto e^{B_t \times T} \quad (20b)$$

169 where P_t and B_t are constants. P_t is commonly assumed to equal 0.0663 [Eppley, 1972].
 170 Substituting equations (20a) and (20b) into equation (19) yields:

$$\sqrt{NCP^*} = a_4 \times \sqrt{e^{P_t \times T}} \times \sqrt{I_m(0)} + a_3 \times \sqrt{e^{B_t \times T}} \times \sqrt{MLD} \quad (21)$$

171 where $a_3 = -\sqrt{\frac{K_I^w}{k_c}}$ and $a_4 = \sqrt{\frac{N_m}{k_c}}$. The NCP^* model for $0 \leq MLD < MLD_{C_{max}^*}$ is not discussed
 172 here, because we do not have data with very shallow MLD to constrain and evaluate the model.
 173 The derivation of the model can be found in the supplementary material.

174 2.5. Comparison to observations

175 2.5.1 Data products

176 We assess the performance of our modeled upper bound on carbon export using a global
 177 dataset of MLD, PAR, sea surface temperature (SST), O_2/Ar -derived NCP, and export
 178 production derived from sediment traps and ^{234}Th (see supplementary material). MLD was



179 derived from global Argo profiles (Global Ocean Data Assimilation Experiment;
180 <http://www.usgodae.org/>) and CTD casts (National Oceanographic Data Center;
181 <https://www.nodc.noaa.gov/>). PAR was downloaded from the NASA ocean color website
182 (<https://oceancolor.gsfc.nasa.gov/>). The NCP estimates are based on a compilation of O₂/Ar
183 measurements from *Li and Cassar* [2016], *Li et al.* [2016], *Shadwick et al.* [2015], and *Martin et*
184 *al.* [2013]. The POC export production estimates were obtained from the recently compiled
185 dataset of *Mouw et al.* [2016]. These estimates were adjusted to reflect a flux at the base of
186 mixed layer using the Martin curve of organic carbon attenuation with depth [*Martin et al.*,
187 1987]. The constants k_c and K_I^w in equation (10) were derived assuming a carbon to chlorophyll
188 a ratio of 90 [*Arrigo et al.*, 2008] and an empirical linear relationship between K_I and
189 chlorophyll a concentration (see Figure S3), calculated based on the NOMAD dataset [*Werdell*
190 *and Bailey*, 2005]. k_m^l was set at 4.1 Einstein m⁻² d⁻¹ following *Behrenfeld and Falkowski* [1997].
191 In our estimation of the upper bound on carbon export, we set N_m to 1 in the NCP^* calculations.

192 2.5.2 Results and discussion

193 Overall, we find that NCP^* calculated using published parameters [*Laws et al.*, 2000] does a
194 good job of enveloping carbon export observations reported in the literature (Figure 3(A)).
195 Samples on the NCP^* envelope (upper bound) are likely regulated by light availability.
196 Conversely, points below the upper bound may be nutrient or in some cases light limited. As
197 expected, NCP^* increases with μ^* and decreases with r_{HR} . Model parameters $a_1 = -1.80$ and
198 $a_2 = 21.38$ (equation (19)) provide the best fit to the O₂/Ar-NCP and MLD estimates. When
199 accounting for the effect of T on μ^* and r_{HR} , model constants $a_3 = -1.66$ and $a_4 = 20.40$
200 (equation (21)) best fit the O₂/Ar-NCP, SST and MLD observations.



201 Our results show that NCP^* decreases faster with increasing MLD in warmer waters (Figure
 202 3(B)), because the term $a_3 \times \sqrt{e^{B_t \times T}}$ in equation (21) is negative and negatively correlated to T .
 203 This temperature effect contributes to part of the relationship between export production and
 204 MLD in Figure 3(A). Interestingly, NCP^* increases with T in colder waters and shallow mixed
 205 layers. This is because NCP^* reflects the balance between productivity ($a_4 \times \sqrt{e^{P_t \times T}} \times \sqrt{I_m(0)}$)
 206 and heterotrophic respiration ($a_3 \times \sqrt{e^{B_t \times T}} \times \sqrt{MLD}$). In a shallow cold mixed layer, the change
 207 in productivity with T ($\frac{d(a_4 \times \sqrt{e^{P_t \times T}} \times \sqrt{I_m(0)})}{dT} = \frac{P_t}{2} \times a_4 \times \sqrt{e^{P_t \times T}} \times \sqrt{I_m(0)}$) is greater than that of
 208 heterotrophic respiration ($\frac{d(a_3 \times \sqrt{e^{B_t \times T}} \times \sqrt{MLD})}{dT} = \frac{B_t}{2} \times a_3 \times \sqrt{e^{B_t \times T}} \times \sqrt{MLD}$). These results could
 209 explain part of the variability in the relationship between NCP and SST reported in previous
 210 studies [Li and Cassar, 2016]. Our NCP^* model does not perform as well in warmer deep mixed
 211 layers, where high variability in export ratio maxima have also been reported [Cael and Follows,
 212 2016]. This may stem from uncertainties in observations, the differing relationship between T ,
 213 μ^* , and r_{HR} at high temperature, and/or violations of our assumptions (see caveats and
 214 limitations).

215 Several recent studies have explored the relationship of NCP to oceanic parameters based on
 216 various statistical approaches [Cassar *et al.*, 2015; Chang *et al.*, 2014; Huang *et al.*, 2012; Li and
 217 Cassar, 2016; Li *et al.*, 2016]. Our model can shed some light into the mechanisms driving some
 218 of these patterns. To that end, we substitute equation (15) into equation (8):

$$NCP(0, MLD) = C \times MLD \times \left(\frac{1 - e^{-K_I \times MLD}}{K_I \times MLD} \times \mu^* - r_{HR} \right) \quad (22)$$

219 Rearranging equation (22):

$$NCP_B = \frac{NCP(0, MLD)}{C \times MLD} = \frac{1}{I_0 + k_m^I} \times N_m \times \mu_{max} \times PAR_{ML} - r_{HR} \quad (23)$$



220 where NCP_B is the biomass-normalized volumetric NCP, PAR_{ML} is the average PAR in the
 221 mixed layer ($PAR_{ML} = \frac{1 - e^{-K_I \times MLD}}{K_I \times MLD} \times I_0$), and $\frac{1}{I_0 + k_m^I} \times N_m \times \mu_{max}$ and $-r_{HR}$ correspond to the
 222 slope and offset, respectively. The scatter in the relationship between chlorophyll-normalized
 223 volumetric NCP and PAR_{ML} , as reported in previous studies [Bender *et al.*, 2016], can likely be
 224 explained by the effect of temperature and the availability of nutrient and light (among other
 225 properties) on the slope and offset of equation (23). Equation (22) can also be reorganized to
 226 assess how environmental conditions may impact the export ratio (ef):

$$ef = \frac{NCP(0, MLD)}{NPP(0, MLD)} = 1 - \frac{K_I \times MLD}{1 - e^{-K_I \times MLD}} \times \frac{1}{N_m} \times \frac{1}{I_m(0)} \times \frac{r_{HR}}{\mu_{max}} \quad (24)$$

227 where $\frac{r_{HR}}{\mu_{max}}$ is proportional to $e^{(B_t - P_t) \times T}$. Equation (24) is consistent with multiple studies which
 228 predict decreasing ef with increasing temperature [Cael and Follows, 2016; Dunne *et al.*, 2005;
 229 Henson *et al.*, 2011; Laws *et al.*, 2000; Li and Cassar, 2016]. In fact, equation (5) of Cael and
 230 Follows [2016] can easily be derived from equation (24) (see supplementary material). Equation
 231 (24) also highlights that a multitude of factors may confound the dependence of ef on
 232 temperature (including varying MLD, light attenuation, and availability of nutrient and light).
 233 This again may explain some of the conflicting observations recently reported in the literature
 234 (e.g., Maiti *et al.* [2013]), where the effect of temperature may be masked by changes in
 235 community composition [Britten *et al.*, 2017; Henson *et al.*, 2015]. One therefore needs to
 236 account or correct for the multitude of confounding factors when predicting the effect of a given
 237 environmental condition (e.g., temperature, mineral ballast, and NPP) on the export ratio.

238 3. Spatial distribution of the upper bound on carbon export

239 We estimate the global distribution of the upper bound of carbon export using equation (19)
 240 and climatological monthly MLD and PAR. In general, NCP^* is high in low latitudes and low in



241 the North Atlantic and Antarctic Circumpolar Current (ACC) in the Southern Ocean (Figure
242 4(A)). As expected, this spatial pattern is controlled by MLD (see Figure S1). Satellite-derived
243 estimates of NCP [Li and Cassar, 2016] are approximately 10% of global NCP^* , reflecting the
244 high degree of nutrient limitation in the oceans. We also derive a global NCP^* map using
245 equation (21), and find that the global NCP^* estimate is very sensitive to the temperature
246 dependence of r_{HR} . For example, decreasing the B_t in $r_{HR} \propto e^{B_t \times T}$ from 0.11 to 0.08 (as used in
247 Rivkin and Legendre [2001] and Lopez-Urrutia et al. [2006]) increases the global NCP^* budget
248 from 87 to 322 Pg C yr⁻¹. Large differences in NCP^* in low-latitudes in great part explain this
249 change. In light of the large uncertainties in the relationship between r_{HR} and T [Cael and
250 Follows, 2016; Lopez-Urrutia et al., 2006], we hereafter only discuss NCP^* estimates derived
251 from equation (19).

252 To estimate how close export production is to its upper bound, we calculate the ratio of
253 export production to NCP^* (f_{pt}). Low f_{pt} regimes represent ecosystems likely regulated by
254 nutrient availability (i.e., ecosystems that have not reached their full export potential based on
255 MLD). As expected, low latitude and subtropical regions have low f_{pt} (Figure 4(B)). High f_{pt}
256 regimes represent ecosystems which have reached their full light potential, and are therefore less
257 likely to respond to nutrient addition because of light limitation (e.g., North Atlantic and ACC
258 (Figure 4(B))). In these regions, especially the subantarctic region, f_{pt} is high in the spring
259 (Figure 4(C)) and decreases in the summer (Figure 4(D)), suggesting that export production is
260 likely co-limited by nutrient and light availability. This may in part explain the lower response to
261 iron fertilization in the subantarctic region where substantial increases in surface chlorophyll
262 were only observed in regions with shallower mixed layers [Boyd et al., 2007; Boyd et al., 2000;
263 de Baar et al., 2005].



264 Also shown in Figure 4 are the biological pump efficiency and export ratio ef (panels 4E and
265 4F, respectively). These various proxies reflect different components of the biological pump.
266 Whereas f_{pt} reflects the export potential based on current MLD and light availability, the
267 biological pump efficiency reflects the potential as derived from nutrient distribution in the
268 oceans, estimated from the extent of nutrient removal from the surface ocean [Sarmiento and
269 Gruber, 2006] or the proportion of regenerated nutrients at depth [Ito and Follows, 2005]. A
270 revised estimate of the global biological pump efficiency, estimated based on the proportion of
271 regenerated to total nutrients (preformed + regenerated) at depth is around 30-35% [Duteil *et al.*,
272 2013]. The ef ratio on the other hand describes how much of production is exported as opposed
273 to recycled in the surface [Dunne *et al.*, 2005]. The ultra-oligotrophic subtropical waters have a
274 low export ratio, a strong biological pump efficiency with exhaustion of nutrients at the ocean
275 surface, and therefore have not reached their full light potential (low f_{pt}). The seasonal pattern
276 of f_{pt} in the subantarctic region suggests that the low biological pump efficiency is the result of
277 light limitation in the austral spring and nutrient (likely Fe) and light limitation in the austral
278 summer.

279 4. Caveats and limitations

280 A multitude of uncertainties, simplifications, and approximations in our model and field
281 observations may explain some of the discrepancies between the predicted and observed NCP^* .
282 Among others:

- 283 • Phytoplankton biomass concentration (C) may vary with depth in the mixed layer,
284 especially for water columns experiencing varying degrees of turbulent mixing. In
285 addition, MLD is not always the best proxy of light availability with mixing layer in



286 some cases deviating from the mixed layer [Franks, 2015; Huisman *et al.*, 1999]. The
287 factors defining the MLD also vary in different oceanic regions.

288 • For simplicity, we model the dependence of photosynthesis on irradiance assuming
289 Michaelis-Menten kinetics, which does not account for photoinhibition. More accurate
290 models can be found in other studies [Platt *et al.*, 1980]. Due to optional absorption, K_I
291 also varies with depth in the mixed layer. Additionally, the linear relationship between K_I
292 and C is influenced by CDOM, NAP, and other environmental factors (e.g., solar zenith
293 angle) [Gordon, 1989].

294 • μ_{max} and r_{HR} are influenced by environmental factors other than temperature, including
295 community structure.

296 • NCP may underestimate export production when accompanied by a decrease in the
297 inventory of organic matter in the mixed layer (see introduction and equation (2)).

298 • Our field observations are limited, mostly focusing on the spring and summer seasons,
299 and harbor significant uncertainties. Descriptions of these uncertainties are presented in
300 other studies [Bender *et al.*, 2011; Cassar *et al.*, 2014; Jonsson *et al.*, 2013].

301 • Finally, our study is only relevant to the mixed layer. It does not account for productivity
302 below the mixed layer, which can be important in some regions such as the subtropical
303 ocean.

304 5. Conclusions

305 In this study, we derived a mechanistic model of an upper bound on carbon export (NCP^*) based
306 on the metabolic balance between photosynthesis and respiration of the plankton community.

307 The upper bound is a positively skewed bell-shaped function of mixed layer depth (MLD). At
308 low temperatures, the upper bound decreases with temperature if mixed layers are deep, but



309 increases with temperature if mixed layers are shallow. We used this model to derive a global
310 distribution of an upper bound on carbon export as a function of MLD, which shows high values
311 in low latitudes and low values in high latitudes due to deep MLD. To examine how current
312 export production compares to this upper bound in the world's oceans, we calculated the ratio of
313 satellite export production estimates to the upper bound derived by our model. High ratios of
314 export production to NCP^* in the North Atlantic and ACC indicate that export production in
315 these regions is likely co-limited by nutrient and light availability. Overall, our results may
316 explain differences in carbon export measured during past iron fertilization experiments (e.g.,
317 subantarctic and polar regions), inform future iron fertilization experiments, and help in the
318 development of remotely-sensed carbon export models.

319 **Acknowledgements**

320 We would like to acknowledge NASA GSFC for processing and distributing PAR and SST
321 products (<http://oceancolor.gsfc.nasa.gov/>). Global Argo temperature-salinity profiling floats
322 were downloaded from <http://www.usgodae.org/>. CTD casts were downloaded from National
323 Oceanographic Data Center (<https://www.nodc.noaa.gov/>). N.C. was supported by NSF OPP-
324 1043339. Z.L. was supported by a NASA Earth and Space Science Fellowship (Grant No.
325 NNX13AN85H).

326 **References**

327 Arrigo, K. R., G. L. van Dijken, and S. Bushinsky (2008), Primary production in the Southern
328 Ocean, 1997-2006, *Journal of Geophysical Research-Oceans*, 113(C8).
329 Baker, K. S., and R. C. Smith (1982), Bio-optical classification and model of natural-waters .2,
330 *Limnology and Oceanography*, 27(3), 500-509.
331 Behrenfeld, M. J., and P. G. Falkowski (1997), Photosynthetic rates derived from satellite-based
332 chlorophyll concentration, *Limnology and Oceanography*, 42(1), 1-20.



- 333 Bender, M., B. Tilbrook, N. Cassar, B. F. Jonsson, A. Poisson, and T. Trull (2016), Ocean
334 productivity south of Australia during spring and summer, *Deep-Sea Res*, *112*, 68-78.
- 335 Bender, M. L., S. Kinter, N. Cassar, and R. Wanninkhof (2011), Evaluating gas transfer velocity
336 parameterizations using upper ocean radon distributions, *Journal of Geophysical Research-*
337 *Oceans*, *116*(C2).
- 338 Boyd, P. W., et al. (2007), Mesoscale iron enrichment experiments 1993-2005: Synthesis and
339 future directions, *Science*, *315*(5812), 612-617.
- 340 Boyd, P. W., et al. (2000), A mesoscale phytoplankton bloom in the polar Southern Ocean
341 stimulated by iron fertilization, *Nature*, *407*(6805), 695-702.
- 342 Britten, G. L., L. Wakamatsu, and F. W. Primeau (2017), The temperature-ballast hypothesis
343 explains carbon export efficiency observations in the Southern Ocean, *Geophys Res Lett*,
344 2016GL072378.
- 345 Cael, B. B., and M. J. Follows (2016), On the temperature dependence of oceanic export
346 efficiency, *Geophys Res Lett*, *43*(10), 5170-5175.
- 347 Cassar, N., C. D. Nevison, and M. Manizza (2014), Correcting oceanic O₂/Ar-net community
348 production estimates for vertical mixing using N₂O observations, *Geophys Res Lett*, *41*(24),
349 8961-8970.
- 350 Cassar, N., P. J. DiFiore, B. A. Barnett, M. L. Bender, A. R. Bowie, B. Tilbrook, K. Petrou, K. J.
351 Westwood, S. W. Wright, and D. Lefevre (2011), The influence of iron and light on net
352 community production in the Subantarctic and Polar Frontal Zones, *Biogeosciences*, *8*(2),
353 227-237.
- 354 Cassar, N., S. W. Wright, P. G. Thomson, T. W. Trull, K. J. Westwood, M. de Salas, A.
355 Davidson, I. Pearce, D. M. Davies, and R. J. Matear (2015), The relation of mixed-layer net
356 community production to phytoplankton community composition in the Southern Ocean,
357 *Global Biogeochem Cy*, *29*(4), 446-462.
- 358 Chang, C. H., N. C. Johnson, and N. Cassar (2014), Neural network-based estimates of Southern
359 Ocean net community production from *in situ* O₂/Ar and satellite observation: A
360 methodological study, *Biogeosciences*, *11*(12), 3279-3297.
- 361 Cullen, J. J., and M. R. Lewis (1988), The Kinetics of algal photoadaptation in the context of
362 vertical mixing, *J Plankton Res*, *10*(5), 1039-1063.



- 363 de Baar, H. J. W., et al. (2005), Synthesis of iron fertilization experiments: From the iron age in
364 the age of enlightenment, *Journal of Geophysical Research-Oceans*, 110(C9).
- 365 Dunne, J. P., R. A. Armstrong, A. Gnanadesikan, and J. L. Sarmiento (2005), Empirical and
366 mechanistic models for the particle export ratio, *Global Biogeochem Cy*, 19(4).
- 367 Duteil, O., W. Koeve, A. Oschlies, D. Bianchi, E. Galbraith, I. Kriest, and R. Matear (2013), A
368 novel estimate of ocean oxygen utilisation points to a reduced rate of respiration in the ocean
369 interior, *Biogeosciences*, 10(11), 7723-7738.
- 370 Dutkiewicz, S., M. Follows, J. Marshall, and W. W. Gregg (2001), Interannual variability of
371 phytoplankton abundances in the North Atlantic, *Deep-Sea Res Pt II*, 48(10), 2323-2344.
- 372 Eppley, R. W. (1972), Temperature and phytoplankton growth in the sea, *Fishery Bulletin*, 70(4),
373 1063-1085.
- 374 Eveleth, R., N. Cassar, R. M. Sherrell, H. Ducklow, M. Meredith, H. Venables, Y. Lin, and Z. Li
375 (2016), Ice melt influence on summertime net community production along the Western
376 Antarctic Peninsula, *Deep Sea Research Part II*.
- 377 Franks, P. J. S. (2015), Has Sverdrup's critical depth hypothesis been tested? Mixed layers vs.
378 turbulent layers, *Ices J Mar Sci*, 72(6), 1897-1907.
- 379 Gordon, H. R. (1989), Can the Lambert-Beer law be applied to the diffuse attenuation coefficient
380 of ocean water, *Limnology and Oceanography*, 34(8), 1389-1409.
- 381 Henson, S. A., A. Yool, and R. Sanders (2015), Variability in efficiency of particulate organic
382 carbon export: A model study, *Global Biogeochem Cy*, 29(1), 33-45.
- 383 Henson, S. A., R. Sanders, E. Madsen, P. J. Morris, F. Le Moigne, and G. D. Quartly (2011), A
384 reduced estimate of the strength of the ocean's biological carbon pump, *Geophys Res Lett*,
385 38(4).
- 386 Huang, K., H. Ducklow, M. Vernet, N. Cassar, and M. L. Bender (2012), Export production and
387 its regulating factors in the West Antarctica Peninsula region of the Southern Ocean, *Global
388 Biogeochem Cy*, 26(2).
- 389 Huisman, J., and F. J. Weissing (1994), Light-limited growth and competition for light in well-
390 mixed aquatic environments: An elementary model, *Ecology*, 75(2), 507-520.
- 391 Huisman, J., P. van Oostveen, and F. J. Weissing (1999), Critical depth and critical turbulence:
392 Two different mechanisms for the development of phytoplankton blooms, *Limnology and
393 Oceanography*, 44(7), 1781-1787.



- 394 Ito, T., and M. J. Follows (2005), Preformed phosphate, soft tissue pump and atmospheric CO₂, *J*
395 *Mar Res*, 63(4), 813-839.
- 396 Jonsson, B. F., S. C. Doney, J. Dunne, and M. Bender (2013), Evaluation of the Southern Ocean
397 O₂/Ar-based NCP estimates in a model framework, *J Geophys Res-Bioge*, 118(2), 385-399.
- 398 Laws, E. A., P. G. Falkowski, W. O. Smith, H. Ducklow, and J. J. McCarthy (2000),
399 Temperature effects on export production in the open ocean, *Global Biogeochem Cy*, 14(4),
400 1231-1246.
- 401 Lewis, M. R., J. J. Cullen, and T. Platt (1984), Relationships between vertical mixing and
402 photoadaptation of phytoplankton: Similarity criteria, *Mar Ecol Prog Ser*, 15(1-2), 141-149.
- 403 Li, Z., and N. Cassar (2016), Satellite estimates of net community production based on O₂/Ar
404 observations and comparison to other estimates, *Global Biogeochem Cy*, 30(5), 735-752.
- 405 Li, Z., N. Cassar, K. Huang, H. Ducklow, and O. Schofield (2016), Interannual variability in net
406 community production at the Western Antarctic Peninsula region (1997-2014), *Journal of*
407 *Geophysical Research*.
- 408 Lopez-Urrutia, A., E. San Martin, R. P. Harris, and X. Irigoien (2006), Scaling the metabolic
409 balance of the oceans, *P Natl Acad Sci USA*, 103(23), 8739-8744.
- 410 Maiti, K., M. A. Charette, K. O. Buesseler, and M. Kahru (2013), An inverse relationship
411 between production and export efficiency in the Southern Ocean, *Geophys Res Lett*, 40(8),
412 1557-1561.
- 413 Martin, J. H., G. A. Knauer, D. M. Karl, and W. W. Broenkow (1987), VERTEX: carbon cycling
414 in the northeast Pacific, *Deep-Sea Res*, 34(2), 267-285.
- 415 Martin, P., et al. (2013), Iron fertilization enhanced net community production but not downward
416 particle flux during the Southern Ocean iron fertilization experiment LOHAFEX, *Global*
417 *Biogeochem Cy*, 27(3), 871-881.
- 418 Morel, A., and L. Prieur (1977), Analysis of variations in ocean color, *Limnology and*
419 *Oceanography*, 22(4), 709-722.
- 420 Mouw, C. B., A. Barnett, G. A. McKinley, L. Gloege, and D. Pilcher (2016), Global ocean
421 particulate organic carbon flux merged with satellite parameters, *Earth System Science Data*.
- 422 Platt, T., C. L. Gallegos, and W. G. Harrison (1980), Photoinhibition of photosynthesis in natural
423 assemblages of marine-phytoplankton, *J Mar Res*, 38(4), 687-701.



- 424 Rivkin, R. B., and L. Legendre (2001), Biogenic carbon cycling in the upper ocean: Effects of
425 microbial respiration, *Science*, 291(5512), 2398-2400.
- 426 Sarmiento, J. L., and N. Gruber (2006), Ocean Biogeochemical Dynamics, *Princeton University*
427 *Press, Princeton, New Jersey*.
- 428 Shadwick, E. H., B. Tilbrook, N. Cassar, T. W. Trull, and S. R. Rintoul (2015), Summertime
429 physical and biological controls on O₂ and CO₂ in the Australian Sector of the Southern
430 Ocean, *J Marine Syst*, 147, 21-28.
- 431 Smith, R. C., and K. S. Baker (1978a), Optical classification of natural waters, *Limnology and*
432 *Oceanography*, 23(2), 260-267.
- 433 Smith, R. C., and K. S. Baker (1978b), The bio-optical state of ocean waters and remote sensing,
434 *Limnology and Oceanography*, 23(2), 247-259.
- 435 Stange, P., L. T. Bach, F. A. C. Le Moigne, J. Taucher, T. Boxhammer, and U. Riebesell (2017),
436 Quantifying the time lag between organic matter production and export in the surface ocean:
437 Implications for estimates of export efficiency, *Geophys Res Lett*, 44(1), 2016GL070875.
- 438 Sverdrup, H. U. (1953), On conditions for the vernal blooming of phytoplankton, *Journal du*
439 *Conseil International pour l'Exploration de la Mer*, 18, 287-295.
- 440 Tortell, P. D., H. C. Bittig, A. Kortzinger, E. M. Jones, and M. Hoppema (2015), Biological and
441 physical controls on N₂, O₂, and CO₂ distributions in contrasting Southern Ocean surface
442 waters, *Global Biogeochem Cy*, 29(7), 994-1013.
- 443 Volk, T., and M. I. Hoffert (1985), Ocean Carbon Pumps: Analysis of relative strengths and
444 efficiencies in ocean-driven atmospheric CO₂ changes, in *The Carbon Cycle and*
445 *Atmospheric CO₂: Natural Variations Archean to Present*, *Geophys. Monogr. Ser.*, edited by
446 *E.T. Sundquist and W. S. Broecker, AGU, Washington, D. C., 1985.*, 32, 99-110.
- 447 Werdell, P. J., and S. W. Bailey (2005), An improved in-situ bio-optical data set for ocean color
448 algorithm development and satellite data product validation, *Remote Sensing of Environment*,
449 98(1), 122-140.
- 450 White, P. A., J. Kalf, J. B. Rasmussen, and J. M. Gasol (1991), The effect of temperature and
451 algal biomass on bacterial production and specific growth rate in fresh water and marine
452 habitats, *Microbial Ecol*, 21(2), 99-118.
- 453

454 **Table 1.** Model symbols, abbreviations, and units

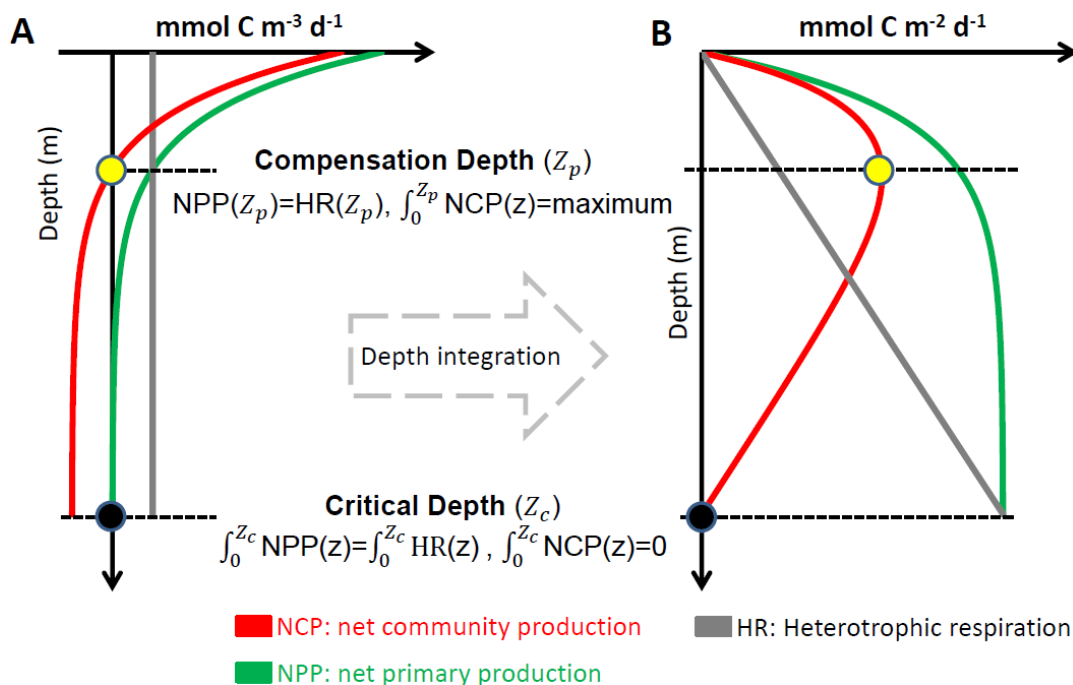
Symbol	Description	Units
MLD	Mixed layer depth	m
$MLD_{c_{max}^*}$	Maximum MLD corresponds to maximum achievable autotroph's biomass concentration	m
z	Depth	m
Z_c	Critical depth	m
Z_p	Compensation depth	m
$GPP(0,z)$	Gross primary production	$\text{mmol C m}^{-2} \text{ d}^{-1}$
$NPP(z)$	Net primary production at depth z	$\text{mmol C m}^{-3} \text{ d}^{-1}$
$NPP(0,z)$	Net primary production above depth z	$\text{mmol C m}^{-2} \text{ d}^{-1}$
$NCP(z)$	Net community production at depth z	$\text{mmol C m}^{-3} \text{ d}^{-1}$
$NCP(0,z)$	Net community production above depth z	$\text{mmol C m}^{-2} \text{ d}^{-1}$
$HR(z)$	Heterotrophic respiration at depth z	$\text{mmol C m}^{-3} \text{ d}^{-1}$
$HR(0,z)$	Heterotrophic respiration above depth z	$\text{mmol C m}^{-2} \text{ d}^{-1}$
NCP^*	The maximum NCP for a given MLD (upper bound on carbon export)	$\text{mmol C m}^{-2} \text{ d}^{-1}$
NCP_B	NCP normalized to autotroph's biomass inventory in the mixed layer	d^{-1}
ef	Export ratio	unitless
f_{pt}	Ratio of satellite export production estimates to the upper bound on carbon export	unitless
N	Nutrient concentration	mmol m^{-3}
k_m^N	Half-saturation constant for nutrient concentration	mmol m^{-3}
N_m	Nutrient effect on phytoplankton grow $N_m = \frac{N}{N+k_m^N}$	unitless
PAR	Photosynthetically active radiation	$\text{Einstein m}^{-2} \text{ d}^{-1}$
I_0	Photosynthetically active radiation just beneath water surface	$\text{Einstein m}^{-2} \text{ d}^{-1}$
$I(z)$	Photosynthetically active radiation at depth z	$\text{Einstein m}^{-2} \text{ d}^{-1}$
k_m^I	Half-saturation constant for irradiance	$\text{Einstein m}^{-2} \text{ d}^{-1}$
$I_m(z)$	Light effect on phytoplankton grow at depth z , $I_m(z) = \frac{I(z)}{I(z)+k_m^I} = \frac{I_0 \times e^{-K_I \times z}}{I_0 \times e^{-K_I \times z} + k_m^I}$	unitless
$I_m(0,z)$	Integrated light effect on phytoplankton grow above depth z , $I_m(0,z) = -\frac{1}{K_I} \times \ln \left(\frac{I_0 \times e^{-K_I \times z} + k_m^I}{I_0 + k_m^I} \right)$	unitless
PAR_{ML}	Average PAR in the mixed layer ($PAR_{ML} = \frac{1-e^{-K_I \times MLD}}{K_I \times MLD} \times I_0$)	$\text{Einstein m}^{-2} \text{ d}^{-1}$
μ	Phytoplankton growth rate	d^{-1}
μ_{max}	Maximum phytoplankton growth rate	d^{-1}
r_{HR}	Heterotrophic respiration ratio	d^{-1}
K_I	Diffusion attenuation coefficient ($K_I = K_I^w +$	m^{-1}



	K_I^{nw})	
K_I^w	Diffusion attenuation coefficient due to water	m^{-1}
K_I^{nw}	Diffusion attenuation coefficient due to optically active components	m^{-1}
k_c	Specific attenuation coefficient for irradiance	$m^2 \text{ mmol}^{-1}$
C	Phytoplankton biomass concentration	mmol m^{-3}
C^*	Phytoplankton biomass concentration that maximizes NCP	mmol m^{-3}
C_{max}^*	Maximum achievable autotroph's biomass concentration	mmol m^{-3}
POC	Particulate organic carbon	mmol m^{-3}
DOC	Dissolved organic carbon	mmol m^{-3}
CDOM	Colored dissolved organic matter	m^{-1}
NAP	Non-algal particles	mmol m^{-3}
T	Temperature	$^{\circ}\text{C}$
P_t	Temperature dependence for phytoplankton grow rate	$^{\circ}\text{C}^{-1}$
B_t	Temperature dependence for heterotrophic respiration ratio	$^{\circ}\text{C}^{-1}$
CO_2	Carbon dioxide	ppmv

455

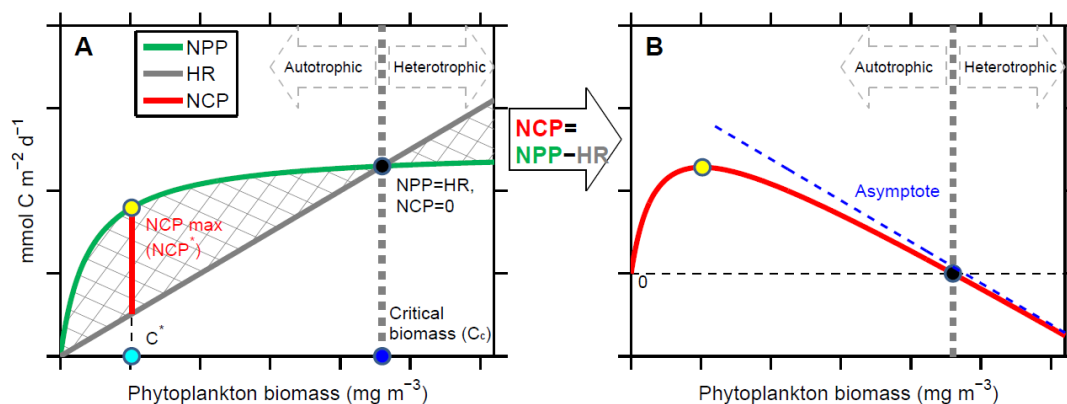
456



457

458 **Figure 1.** Schematic diagram of depth-profiles of net community production (NCP), net primary
 459 production (NPP), and heterotrophic respiration (HR). Yellow and black dots represent the
 460 compensation and critical depths, respectively.

461



462

463 **Figure 2.** Relationship between net primary production (NPP), heterotrophic respiration (HR),

464 net community production (NCP), and phytoplankton biomass concentration (C) for a given

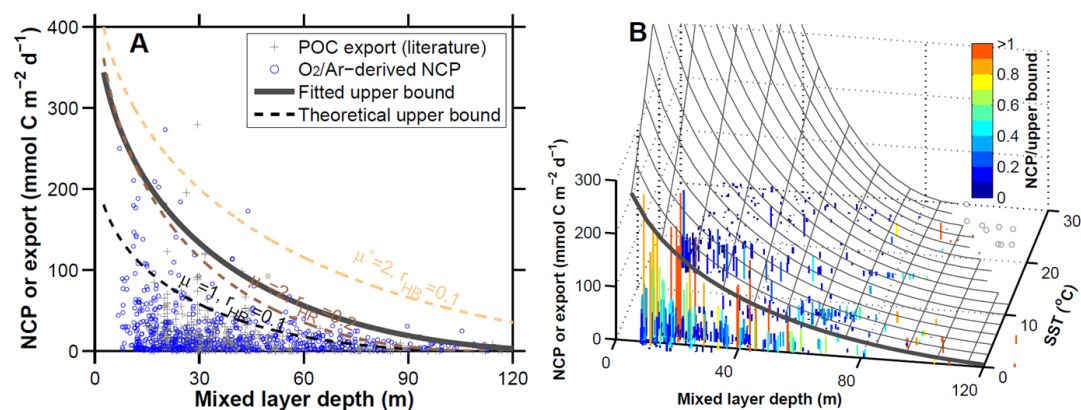
465 mixed layer depth (MLD). Hatched area in panel A represents NCP. The yellow dot represents

466 the maximal NCP (NCP^*) obtainable for a given MLD, with the corresponding phytoplankton467 biomass concentration (C^*) denoted with a cyan dot. NCP on the right of the yellow dot468 decreases with C due to self-shading. Black dot represents depth-integrated $\text{NCP} = 0$ (i.e.,469 $\text{NPP} = \text{HR}$), with the corresponding phytoplankton biomass concentration defined as critical470 biomass (C_c) and denoted with a blue dot. Ecosystems on the left and right of this threshold are

471 net autotrophic and heterotrophic, respectively. The asymptote (dashed blue line) in panel B

472 represents a system dominated by heterotrophic respiration (i.e., $\text{NCP} \approx \text{HR} \gg \text{NPP}$).

473



474

475 **Figure 3.** Envelope of the modeled upper bound on carbon export production compared to field

476 observations as a function of mixed layer depth (MLD) and sea surface temperature (SST).

477 Observations are based on ²³⁴Th and sediment traps estimates of carbon export production and478 O₂/Ar-derived net community production. To account for the effect of PAR on export production,479 both MLD and carbon fluxes are normalized to $I_m(0) = \frac{I_0}{I_0 + k_m}$ (see equations (19) and (21)). (A)480 The thick gray line represents the upper bound fitted to the O₂/Ar-NCP data. Dash-lines

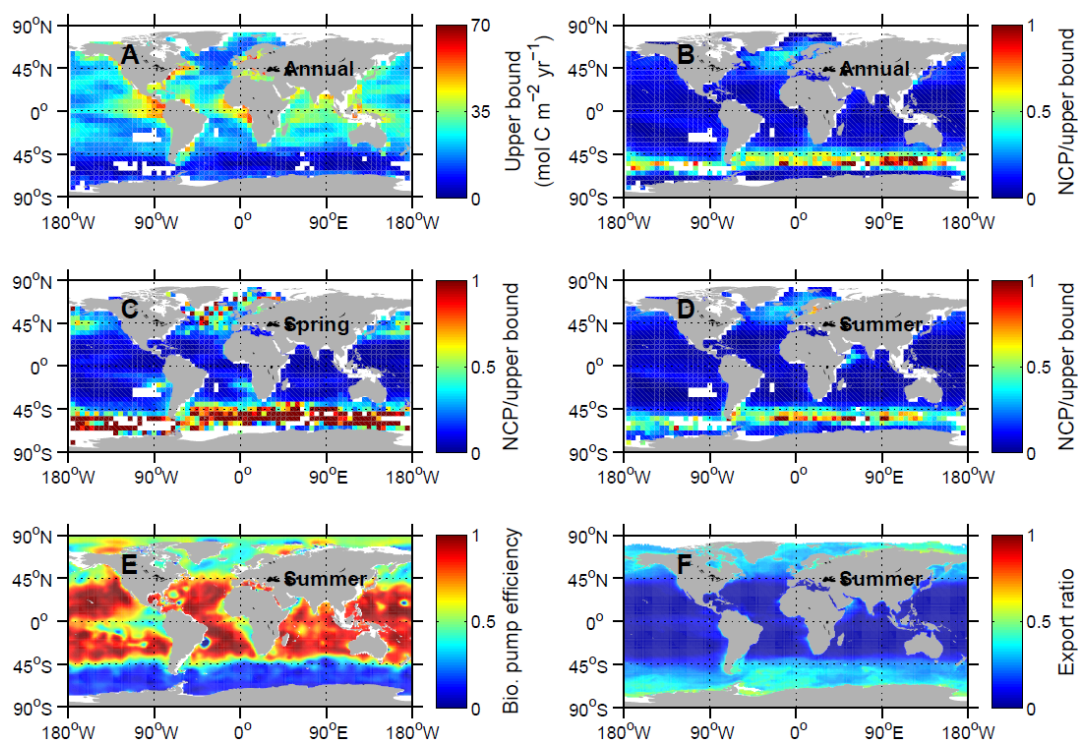
481 represent the upper bounds calculated using parameters available in the literature. (B) Surface

482 representing the envelope of the modeled upper bound of carbon export production as a function

483 of SST and MLD. Bars represent field observations color coded with the ratio of NCP to the

484 upper bound. A stoichiometric ratio of O₂/C=1.4 was used to convert NCP from O₂ to C units485 [Laws, 1991]. The temperature dependence of r_{HR} was modeled as $r_{HR} \propto e^{0.08 \times T}$.

486



487

488 **Figure 4.** (A) Modeled upper bound on carbon export derived from equation (19), (B-D) ratios
489 of satellite export production estimates to the upper bound on carbon export, (E) biological pump
490 efficiency calculated as the difference in nutrient concentrations between surface and depth,
491 normalized to nutrient concentrations at depth [Sarmiento and Gruber, 2006] (nitrate
492 concentration from World Ocean Atlas (<https://www.nodc.noaa.gov/OC5/woa13/>)), and (F)
493 export ratio derived from Dunne *et al.* [2005]. Annual represents annually-integrated value.
494 Spring and summer represent average value in spring and summer, respectively. In the northern
495 hemisphere, spring and summer seasons are defined as March-May and June-August,
496 respectively. In the southern hemisphere, spring and summer seasons are defined as September-
497 November and December-February, respectively.

498